Simulation of the Behavior of 32-Layer Composite Plate for Ballistic Protection

George Ghiocel OJOC[1], Larisa CHIPER TITIRE[1],
Lorena DELEANU*,[1], Cristian MUNTENITA[1], Catalin PIRVU[2]

*Corresponding author
[1]"Dunarea de Jos" University, Faculty of Engineering,
Department of Mechanical Engineering,
111 Domneasca, Galati, Romania,
lorena.deleanu@ugal.ro*
[2]INCAS – National Institute for Aerospace Research "Elie Carafoli",
220 Avenue Iuliu Maniu, Bucharest 061126, Romania,
pirvu.catalin@incas.ro

DOI: 10.13111/2066-8201.2022.14.4.8

Received: 20 September 2022/ Accepted: 27 October 2022/ Published: December 2022

Abstract: *This paper presents experimental results and a failure analysis of a composite for ballistic protection. The stratified plate is manufactured at laboratory scale, after a technology designed by the authors. The plates were tested for level FB2, taking into account the standard SR EN 1522:2004 (Windows, doors, shutters and blinds. Bullet resistance. Requirements and classification) and SR EN 1523:2004 (Windows, doors, shutters and blinds. Bullet resistance. Test method) and the results point out that this plate could face more dangerous threats. In order to evaluate the behavior of the plate under the impact characterizing a higher level of threat, the authors uses a FE model and simulated the system bullet – plate for different impact velocities.*

Key Words: *ballistic test, FE model, composite.*

1. INTRODUCTION

Materials for ballistic protection have a complex behavior under impact load and specific processes need to be modeled: nonlinear response to stress, hardening under stress and stress dependence on strain rate, thermal softening, orthotropic response (for composites, especially those made of fabrics), damage by crushing (when including ceramics, glass, concrete), processes involving chemical energy release (when dealing with explosions), failure, phase changes (transition from solid-liquid-gas and vice versa). The modeling of these processes can be done with the help of three components: the state equation, the material strength model and the failure model [1], [2], [3], [4].

2. MATERIALS AND PLATE FABRICATION

The fabric, as a prepeg, is layered into four oriented substrates (0°/+45°/90°/-45°), which assumes that it will have a quasi-isotropic behavior. Trade name is 1200 g/m^2 Quatriaxial Glass Cloth (0°/+45°/90°/-45°), with the code WTVQX1200-1 E-glass, Q1200E10Q [5]. Figure 1

shows the size of the glass fiber yarns and fibers, measured under an scanning electron microscope.

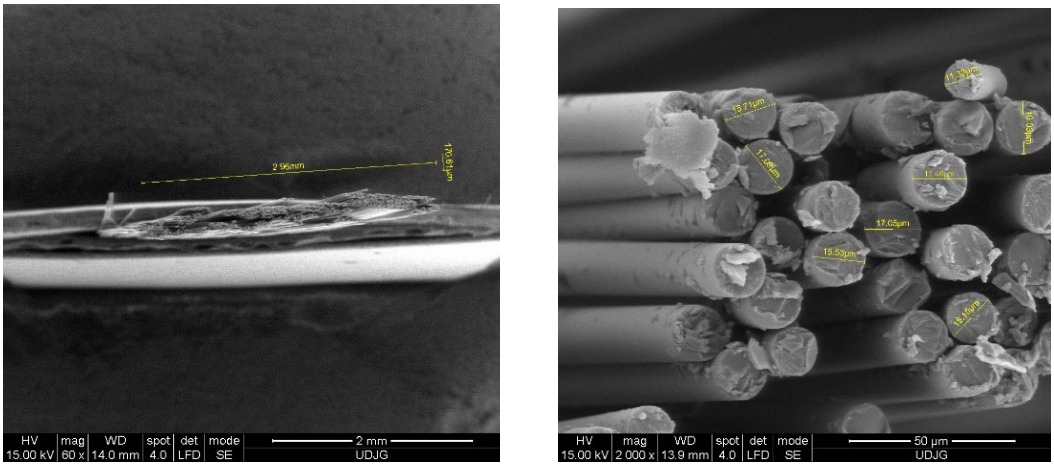

a) Yarn dimensions b) Glass fiber diameter

Fig. 1 Photos of the tested plate made of 32 layer of glass fiber fabrics

The rolls of glass fiber fabric were kept in the laboratory, at a relative humidity of 40-70% and a temperature of 18-30°C, as recommended by the manufacturer.

Polyester, vinyl ester and epoxy resins are compatible with this fabric. The water content is at maximum 0.2% by mass.

Table 1. Typical mechanical and thermal properties of fully cured neat resin

Resin **Biresin® CR82** with hardener **Biresin® CH80-2**			
Tensile strength	ISO 527	MPa	90
Tensile Elasticity Modulus	ISO 527	MPa	3000
Elongation at break	ISO 527	%	5.6
Flexural strength	ISO 178	MPa	130
Flexural Modulus	ISO 178	MPa	3200
Compressive strength	ISO 604	MPa	105
Density	ISO 1183	g/cm^3	1.14
Shore hardness	ISO 868	-	D 85
Impact resistance	ISO 179	kJ/m^2	66

It was selected the two-component resin Biresin® CR82 with hardener CH80-2 (Table 1), from the products offered by the manufacturer Sika Group [6]. The mixing ratio hardener – resin must be followed accurately, as given in the resin data sheet, for optimal results (27:100).

The plates are destinated for light armor for vehicles and protected enclosures. The advantage of this technology is that plates of different thicknesses can be made following the same steps and with characteristics in a narrow range (for example, the fibers mass concentration, allowances of thicknesses etc.).

The cutting process of the fabrics was carried out with the help of an electric scissors, brand Vibromat S-54, with a cutting diameter of the disk having 50 mm, the output power 80W and the maximum cutting height of the layers being 12 mm. Only one layer each was cut.

Table 2. Characteristics of plates made of 32 layers of quadriaxial glass fiber fabrics

No.	Fabric mass	Panel mass	Resin mass*	Fabric/panel mass ratio**	Surface density***	Thickness in 4 points				
						1	2	3	4	average
	[g]	[g]	[g]		[kg/ m^2]	[mm]				
0	1	2	3	4	5	6	7	8	9	10
Panel 1	3320	4506	1186	0.736	36.88	26.89	26.63	25.83	24.60	25.99
Panel 2	3330	4611	1281	0.722	37	25.73	27.41	26.93	26.40	26.62
Panel 3	3220	4400	1180	0.731	35.77	23.94	24.45	24.24	25.63	24.57
Average	**3290**	**4506**	**1216**	**0.729**	**36.55**					**25.73**
Max	3330	4611	1281	0.736	37					
Min	3220	4400	1180	0.722	35.77					
Standard deviation	**49.67**	**86.14**	**46.26**	**0.006**	**0.554**					**0.857**
	1.5%****	1.91%	3.80%	0.82%	1.51%					3.33%

* The resin mass = panel mass – frics mass, meaning (column 2 - column 1)
** Fabric/panel mass ratio = Fabric mass / Panel mass, meaning (column 1/ column 2)
*** Surface density = Panel mass /Panel surface (0.09 m^2)
**** Standard deviation in percentage is calculated as (standard deviation / average value of the same characteristics)*100

Because of the prototype scale of the fabrication, a mixture of 800 g of CR82 resin and 200 g of CH80-2 hardener was mixed for panels with 32 layers.

Weighing the resin components and panels was done with a precision electronic scale. The characteristics of the elaborated panels are given in Table 2.

Analyzing the values, small standard deviations and an almost constant fiber/panel mass ratio are noticed.

The fabrication process has precision, repeatability and robustness. The plates have the dimensions 300 mm x 300 mm.

The fabrication was done in compliance with the norms of safety and health at work, with adequate protective equipment.

The technological process of fabricating the OGe plates includes the following steps:

- cutting the fabric layers (and weighing the cut layers that will be included in each panel);
- making the resin + hardener mixture;
- wax laying-up of the matrix (for an easier extract of the plate after pressing),
- laying-up the liquid matrix and overlapping the layers of fabric;
- pressing, maintaining and controlling the thickness of the panel in press;
- heat treatment, including natural ageing for 7 days and maintenance at 60 °C, for 6 h;
- quality control (weighing, thickness measurement).

Depending on the results of ballistic tests, the technology may be improved in order to reduce the time of manufacturing and control, based on the experience gain in making these sets of panels.

3. EXPERIMENTAL REZULTS AND FAILURE ANALYSIS

Figure 2 and figure 3 present the set of three fires on the same plate for the 32-layers plate with the impact velocity of 375 m/s. The cross sections in Figure 2 were obtained by high-speed dry cutting.

The photos point out the resemblance of hits in plate's behavior and the small number of damaged layer.

There were noticed delamination of superficial layers, cut of fibers as result of bullet penetration through 3…4 layers, delamination due to lateral projectile flattening and compression of the first layers under the stopped projectile.

a) Front view

b) Cross section (with high speed disk, dry regime)

Fig. 2 Photos of the tested plate made of 32 layer of glass fiber fabrics.

a) Fire 1 b) Fire 2 c) Fire 3

Fig. 3 Details of the three fires on the same plate

4. RESULTS OF NUMERICAL SIMULATION AND CONCLUSIONS

The model includes a plate with 32 layers, each layer being considered homogenous and isotropic. Layers are assembled by using the cohesive zero model [7].

Each of the two projectiles is modeled as a two-body bullet, with a "perfectly bonded" jacket-core connection.

The panel has an area of 120 mm x 120 mm. The actual panel, made and tested by the authors, is 300 mm x 300 mm, which allowed to have 3 fires, at a distance between them of 120 mm, in an equilateral triangle.

Due to running time and hardware features, the simulation is run for a single hit on a smaller surface (120 mm x 120 mm), being sufficient to cover the delamination process for a single fire, as observed on actual panels.

The bullet in Figure 4a was drawn after [8] and the bullet in Figure 4b is drawn after [9].

The connection between layers is "bonded", with the condition of "breakable" detachment, this being conditioned by exceeding a value for tensile stress and shear stress, introduced with the value of 90 MPa for traction stress and with the value of 60 MPa for the shear stress, characteristic for the resin attaching the layers in the actual panel.

In this model, the breakable option was set with the "Stress Criteria", and then the connection can be broken during the analysis [10]. The breaking criterion is defined as follows [11]:

$$\left(\frac{\sigma_n}{\sigma_n^{limit}}\right)^n + \left(\frac{|\sigma_s|}{\sigma_s^{limit}}\right)^m \geq 1 \quad (1)$$

where σ_n^{limit} is the value for the limit at break for normal stress (in this model n is the value of the exponent in the relation (1), for the ratio of normal stresses n = 1), σ_s^{limit} is the value for the shear limit at break, m being the value of the exponent in relation (1), for the shear stress ratio.

The interaction between bodies is considered with friction, the coefficient of friction being constant, set at COF = 0.1. The value of coefficient of friction in case of impact is difficult to measure, the tests reported in the literature being done for relatively lower velocities than those in reality and taking into account only the slip between two bodies. The range found in the literature is from values below 0.1 to 0.4 [12], [13].

In reality, during the impact process, the coefficient of friction is not constant and depends on the pair of materials between which the movement takes place and the stress in the normal direction.

In order to reduce the running time, the bullet was brought as close as possible to the panel, the distance between the tip of the bullet and the plate being 0.25 mm.

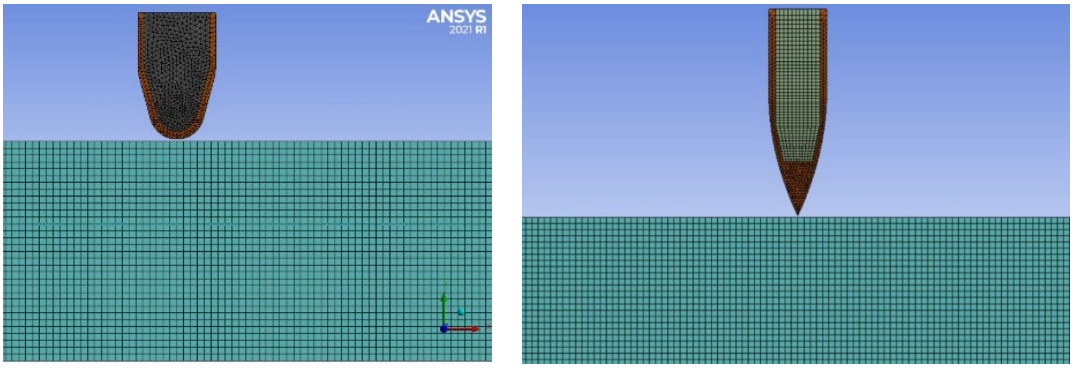

a) with 9 mm FMJ b) with 7.62 projectile

Fig. 4 Meshing of the system

The discretization network was done after a documentation on the subject, from which it resulted that the element size and the discretization style are important, but must be adapted to the particular case that is modeled [14].

For the bullet, a tetrahedral network with at least two elements on the thickness of the jacket was used, obtained from an initial discretization, over which a discretization with 3 spheres of influence, with a radius of 5 mm, 10 mm and 15 mm (Fig. 5a) and for the second bullet a discretization with 3 spheres of influence, with a radius of 15 mm, 20 mm and 25 mm (Fig. 5b), was added in order to have a relatively controlled and smaller growth of network elements.

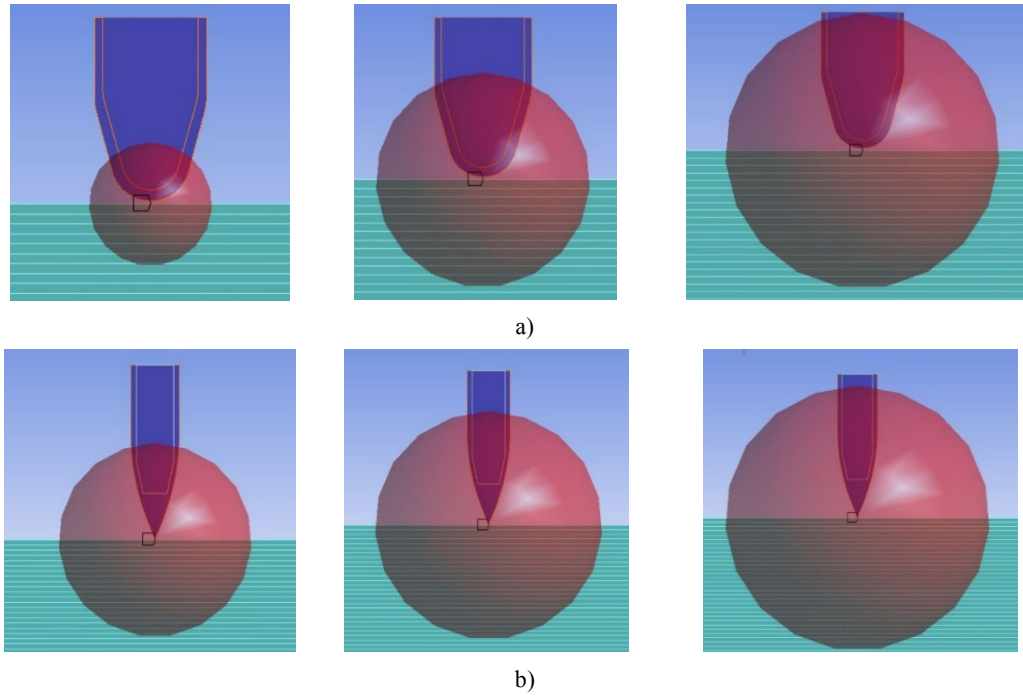

a)

b)

Fig. 5 Differentiated zones for the projectile mesh

For the 5 mm sphere, the size of the element was 0.35 mm, for the next sphere, it was 0.45 mm and for the largest sphere, 0.55 mm, respectively).

Each layer of the panel has a thickness of 0.8 mm (like the layer of the actual panel), with one element per thickness.

The initial condition is the projectile velocity, just before hitting the plate. Boundary conditions involve the lateral fixing of the panel. Each layer is fixed on its lateral side surface.

The model contains a plane of symmetry that passes through the center of the plate square and this is parallel to one side of the panel (it also contains the longitudinal section of the projectile).

The model is considered as isothermal for two reasons. Explicit Dynamics does not support adiabatic models and research studies reported that in this range of impact velocities, 300 m/s to 700 m/s, the thermal influence may be neglected in impact failure, especially for materials that are heat-resistant as glass fiber fabrics and some epoxy resins.

In these simulations, the Johnson-Cook [15] model was used for the core material (a lead alloy) and the jacket material (a brass alloy), based on the experimental data obtained by [16], [17], [18] (Table 3). Each layer of the panel has the mechanical characteristics in Table 4.

The cohesive model zone, with zero thickness (CMZ) was introduced between the layers [19], the name in Explicit Dynamics commands for modeling the resistance of CZM being "Bilinear for interface delamination" (Table 5) [10], the failure criterion being set for "Fracture energies based debonding" (Table 6), for crack opening mode I.

Table 3. Mechanical properties for materials the projectile jacket and core are made of

Property	**Jacket (brass)**	**Core (Lead alloy)**
Density *[kg mm^-3]*	8.45e-6	1.135e-5
Specific heat at constant pressure *[mJ kg^-1 C^-1]*	380	1.288e+5
Young modulus *[MPa]*	90000	16000
Poisson coefficient	0.344	0.44
Temperature *[°C]*	22	22
Constants for Johnson-Cook model		
Initial yield limit *[MPa]*	90	1
Hardening constant *[MPa]*	628	55
Hardening exponent	0.72	9.8e-2
Constant for strain rate	0.266	0.231
Exponentul înmuierii termice	604	221
Melting temperature *[°C]*	927	327.5
Plastic strain rate (/sec)	1	1
Echivalent plastic strain at break	0.4	0.4

Table 4. Mechanical properties of a layer

Property	**Value**
Density *[kg/mm^3]*	1904
Specific heat at constant pressure *[mJ/(kg °C)*	6e+5
Young modulus *[MPa]*	50000
Poisson coefficien	0.3065
Temperature *[°C]*	22
Isotrope bilinear hardening model	
Initial yield limit *[MPa]*	550
Tangent modulus *[MPa]*	10000
Temperature *[°C]*	22
Equivalent plastic strain at break	0.11

Table 5. Parameters for modeling the bilinear strength in interlaminar delamination

Temperature, °C	Maximum normal traction, MPa	Normal displacement jump at completion of debonding, mm	Maximum tangential traction, MPa	Tangential displacement jump at completion of debonding, mm	Ratio
22	70	5	50	0.1	0.3

Table 6. Parameters for energy at break in delamination

Tempe-rature, °C	Maximum normal contact stress, MPa	Critical fracture energy for normal separation, J/m^2	Maximum equivalent tangential contact stress, MPa	Critical fracture energy for tangential slip, J/m^2	Artificial damping coefficient, s
22	100	3000	-	-	0.1

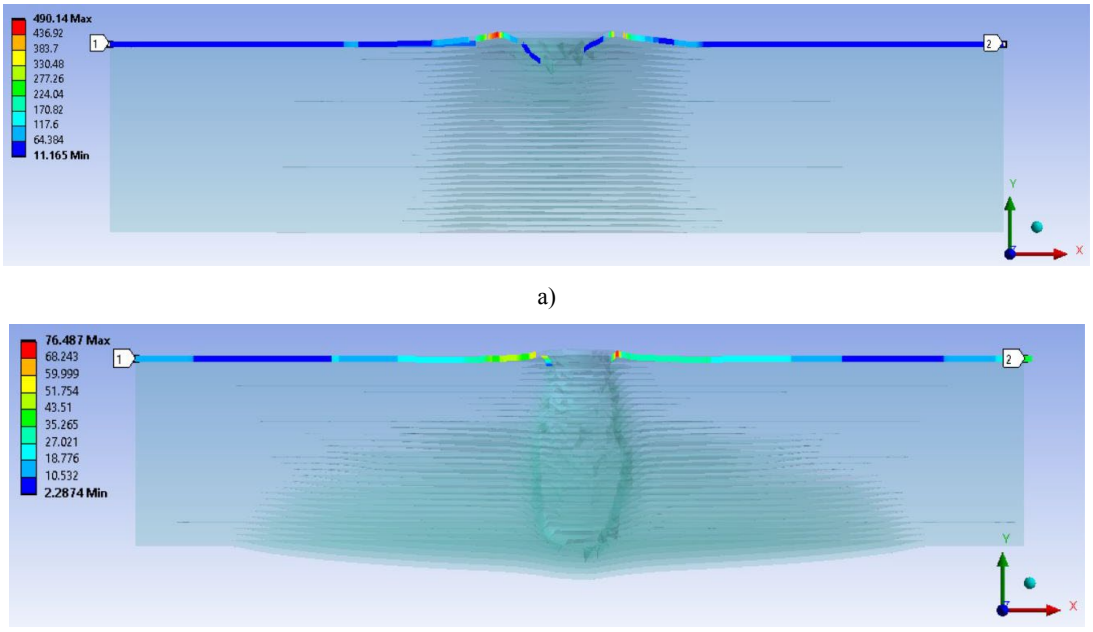

Fig. 6 An exemple of von Mises stress distribution on the first layer of the plate: a) for round nose projectile and b) for pointed nose projectile type 7.72, at the same moment of the simulation (stress in MPa)

The equivalent stress distributions on each layer were analyzed using the "Path" function in Explicit Dynamics (exemples are given in Fig. 6) and compared for different panel thicknesses, obtaining the influence of the number of layers on the evolution of the equivalent stresses over time, on a layer of interest.

Images (moments) belonging to the stages of the impact process can be extracted from the simulation.

Figure 6 presents an exemple of analysing the stress distribution on a layer, pointing out if the layer is broken and where the stress concentrations are located for the analysed moment.

The analysis is based on comparing the impact stages for each case and it points out the difference in failure process, based on graphs of the equivalent stress on several selected layers and on images extracted from run simulations.

In order to make visible the damages in the composite, the projectile is made transparent. Figure 7 present the first moment of the simulation, for three different impact velocities.

The cases with low velocities (a and b) do not have yet broken the first layer, but for the high velocity, there are two or three layers already failed and the shape of the plate around the projectile is different: for round nose, the crater in the plate is greater, a small delamination is visible between layers 1 and 2 and for the pointed projectile the deformation of the first layer is reduced, stress concentrators occur under the pointed nose and delamination is not noticed.

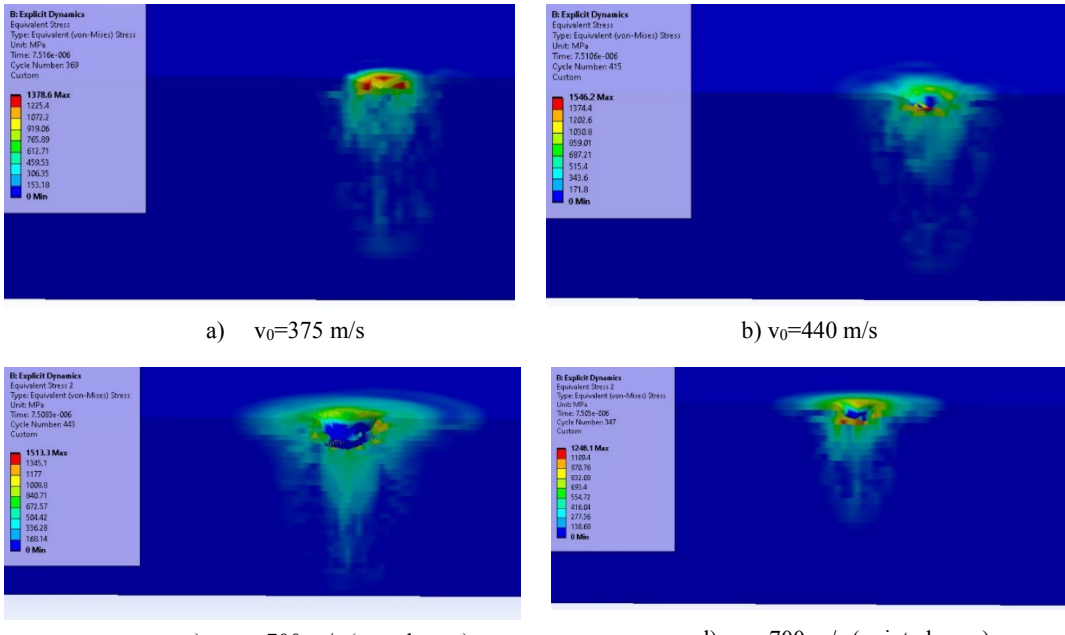

a) v_0=375 m/s b) v_0=440 m/s

c) v_0=700 m/s (round nose) d) v_0=700 m/s (pointed nose)

Fig. 7 32-layers panel at t=7.5×10^{-6} s (the first moment of the simulation) for different impact velocities and with round nose projectile (a, b and c) and with pointed 7.62 projectile (d)

The stressed volume is greater for the round nose projectile. Analysing the first graph in Fig. 8, one may notice layer 1 is broken for v_0=440 m/s and for the cases with v_0=700 m/s. The high values of von Mises stress on layer 1 presumes that in the next moment the layer will break. At t=3.75×10^{-5} s, only the smallest velocity could not break layer 1.

At t=1.5×10^{-4} s, layer 1 has the values for von Mises stress less the strength limit of the layer, the higher values being caused both by the friction between layer and projectile and the layer bending near the projectile.

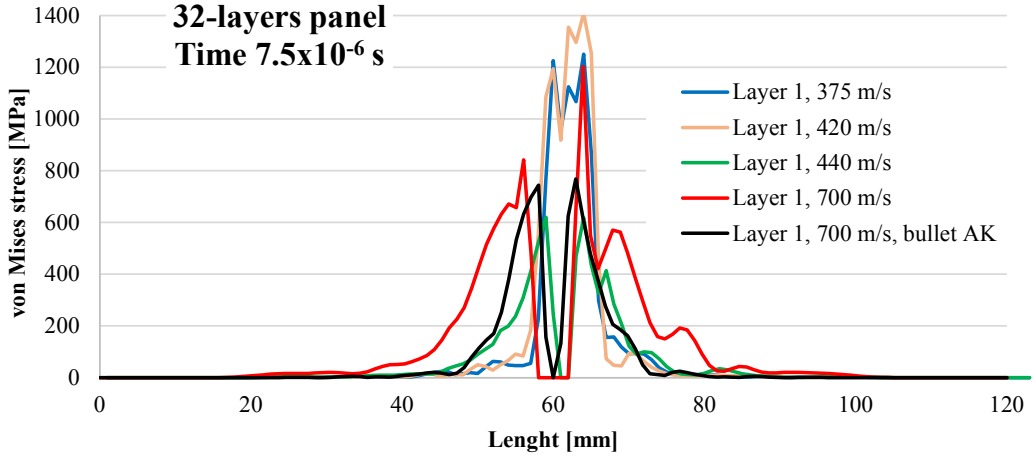

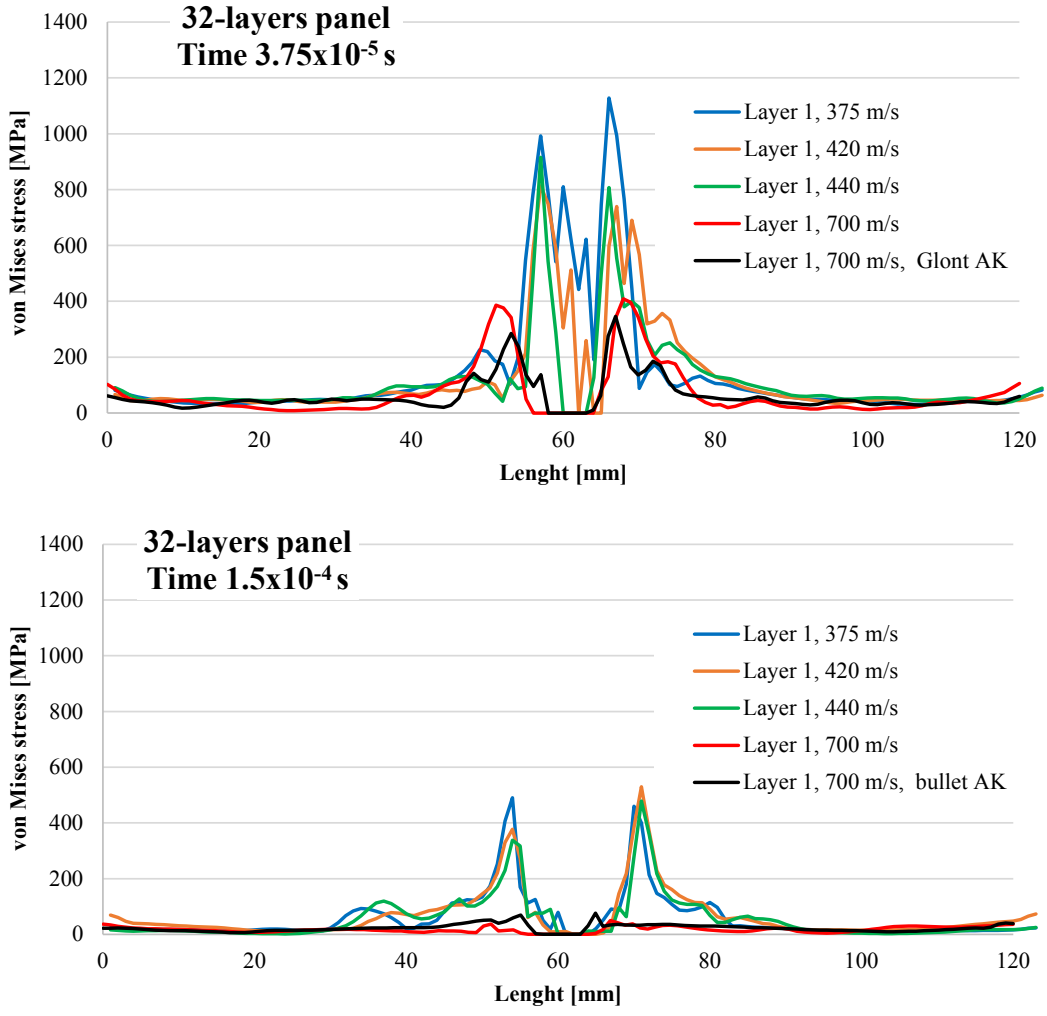

Fig. 8 von Mises stress distributions on layer 1, for different moment of the simulation

The space for comments not being too large, the next figure (Fig. 9) presents the von Mises stress distribution for layer 8, at the same moments as for layer 1.

Layer 8 is more stressed (approx. 600 MPa), at $t=7.5\times10^{-6}$ s, for the round projectile. Layer 8 does not fail for $v_0=375$ m/s till $v_0=440$ m/s, the maximum value for equivalent stress being around 200…300 MPa.

At moment $t=3.75\times10^{-5}$ s, layer 8 failed for both cases with 700 m/s, for the other cases, the maximum stress being around 600 MPa. At $t=1.5\times10^{-4}$ s, all values for the equivalent stress is low, around 200 MPa, thus the impact with breakage is ended for this layer.

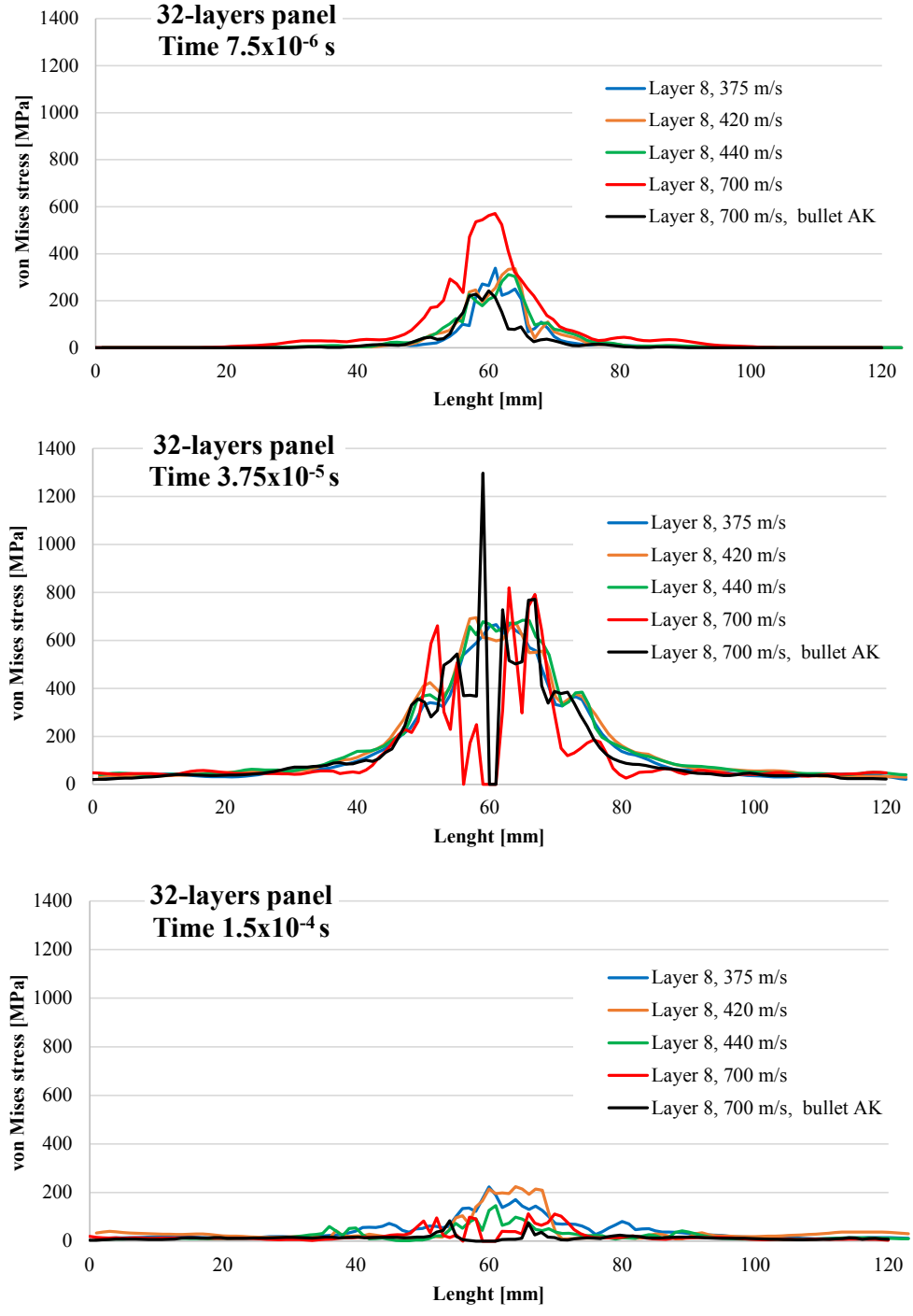

Fig. 9 von Mises stress distributions on layer 8, for different moments of the simulation

The image from simulation points out that at $t=3.75\times10^{-5}$ s and $v_0=700$ m/s, 11 layers have been already failed for the round nose projectile and 9 layers for the pointed projectile. Delamination is visible among almost all broken layers and the orifice shape suggest that the bullet tends to flatten laterally, in the specific shape of a mushroom.

No delamination is visible under the projectile. At the same moment, t=3.75×10^{-5} s, the projectile is flattened on the panel surface and this process is visible on Fig. 10 that presents the actual panel after test at v_0=375 m/s.

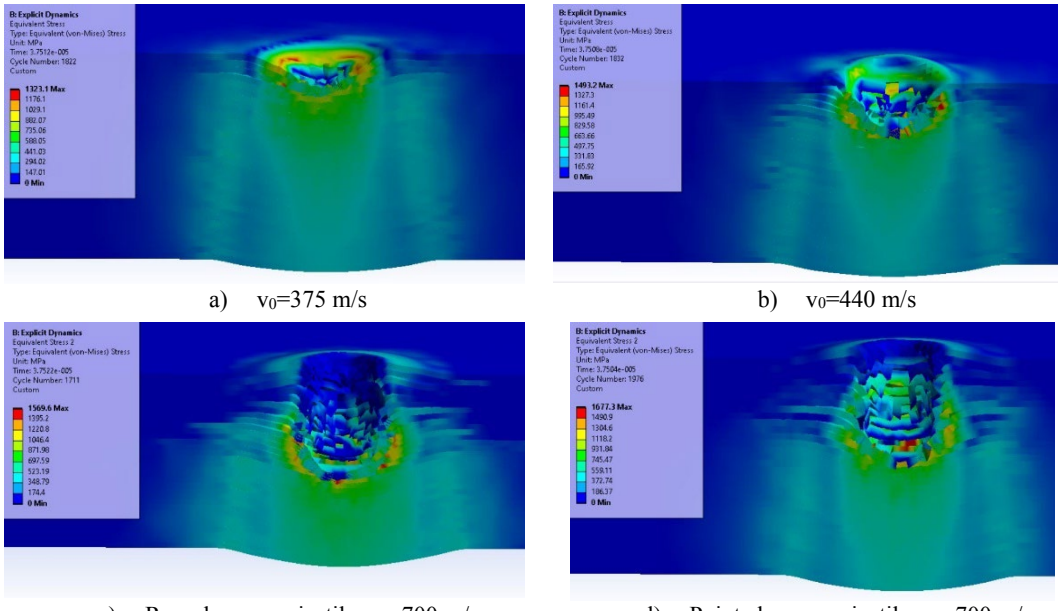

a) v_0=375 m/s b) v_0=440 m/s

c) Round nose projectile, v_0=700 m/s d) Pointed nose projectile, v_0=700 m/s

Fig. 10 32-layers panel at t=3.75×10^{-5} s (the first moment of the simulation) for different impact velocities and with round nose projectile (a, b and c) and with pointed 7.62 projectile (d)

Next analyzed layer is layer 16. At moment t=3.75×10^{-5} s, high values for the stress are given only for v_0=700 m/s, for the round nose, the evolution of the stress on this layer being not so sharp for the pointed projectile, but at 9×10^{-5} s, both projectiles at v_0=700 m/s have broken layer 16 (Fig. 11).

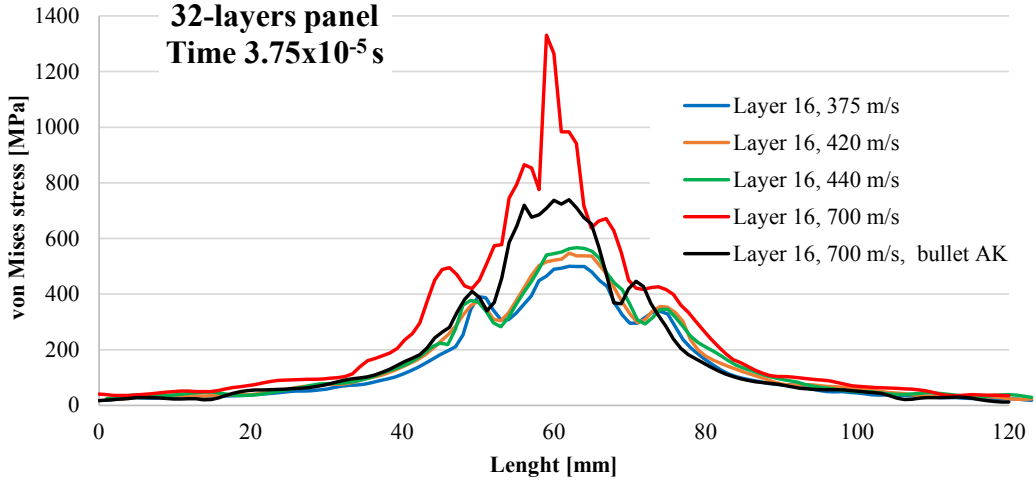

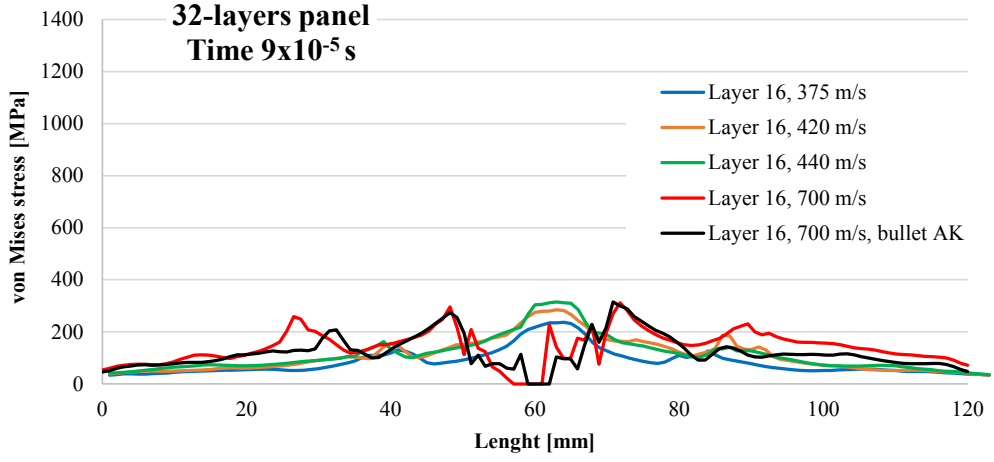

Fig. 11 von Mises stress distributions on layer 16, for different moments of the simulation

Analysing the behavior of layer 24, till the moment 7.5×10^{-5} s, only the pointed projectile rises the stress toward the considered limit at break of the layer and at moment $t=1.5\times10^{-4}$ s, it has already broken the layer 24. The round nose projectile does not break it, at the same moment (Fig. 12).

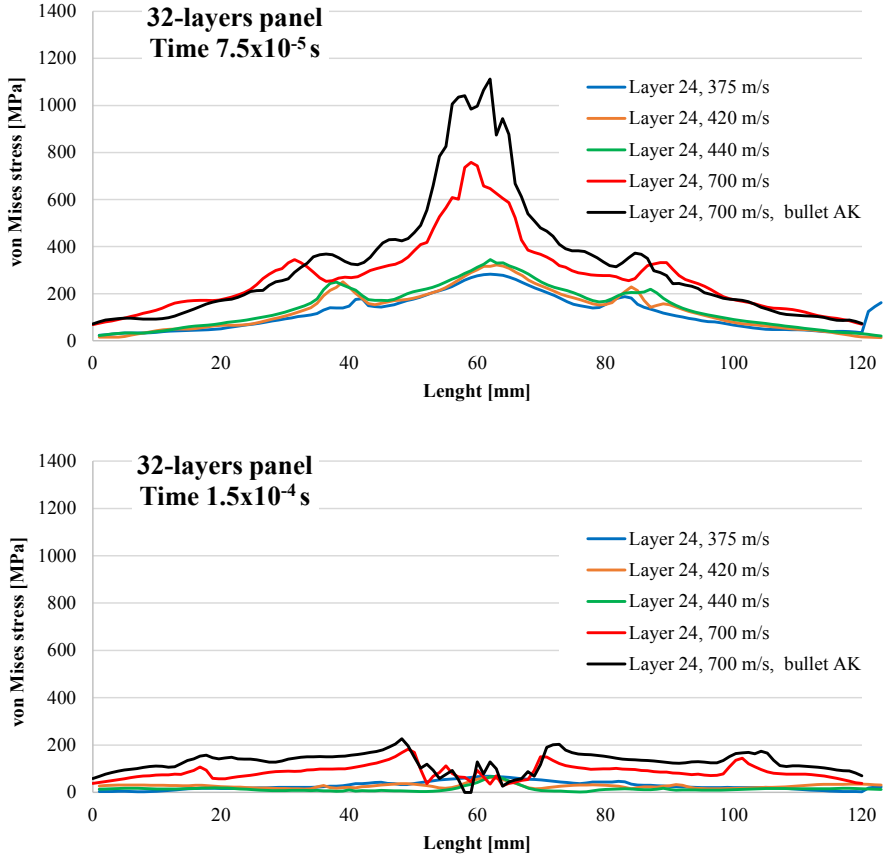

Fig. 12 von Mises stress distributions on layer 24, for different moments of the simulation

On layer 32, the maximum stress is obtained for round nose projectile, at v_0=700 m/s, but bellow the yield limit considered for the layer. Figure 13 presents the equivalent stress distributions at moment t=1.425×10^{-4} s.

Pay attention to the color scale and one may noticed that the maximu values are under the considered yield limit, so the failure of layers does not occur anymore, but delamination could advance due to the bullet deformation and fragmentation.

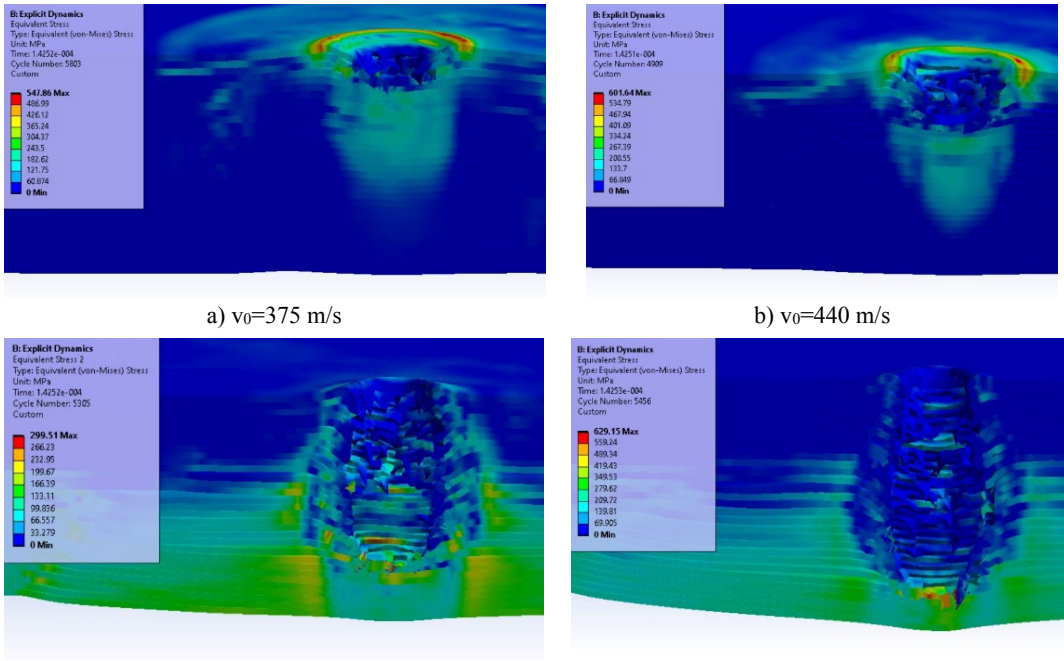

a) v_0=375 m/s

b) v_0=440 m/s

c) v_0=700 m/s (round nose projectile)

d) v_0=700 m/s (pointed nose projectile)

Fig. 13 Images of a moment near the end of the simulation (t=1.425×10^{-4} s). Projectile is transparent

Analyzing these images, it is obvious that pointed projectile damaged more intensively the panel, taking into account the number of broken layers. As the thermal effect was not taken into account in this simulation, the actual panel could behave under two scenarios:

- due to thermal field generated by friction between projectile and layers, it is possible a reduction in the mechanical properties of both metallic alloys of the projectile, meaning that failure also will be reduced,
- this thermal efect will increase the delamination progress and the bending of last resisting layers that could break.

5. CONCLUSIONS

Taking into account that the model was validated by the number of broken layers for v_0=375 m/s, it is a high probability that the 32-layers panel to resist at impact with 7.62 mm projectile (pointed nose), at v_0=700 m/s, but the authors considered that only a percentage of 18.75% intact layers is not recommended for an actual ballistic protection. Thus, simulation helps the designers to start an actual test campaign with panels of 32 layers or more for the threat taken into account. The failure processes in virtual environment were compared to those obtained on the tested panels. The simulation results point out that this 32-layer plate could face more dangerous threats than FB2.

ACKNOWLEDGEMENT

The authors would like to express our deepest gratitude to the Scientific and Organizing Committees of the *10th Conference* "***AEROSPATIAL***" held at the INCAS – National Institute for Aerospace Research "Elie Carafoli", Bucharest, under the aegis of The Romanian Academy for their support for researchers to make known their results.
Also, we would like to extend our sincere thanks to family Vasilca, represented by eng. George Vasilca and eng. Dan Vasilca, that in partnership with the INCAS – National Institute for Aerospace Research "Elie Carafoli", Bucharest, have been encouraging young researchers to participate in a competition for the award "Gheorghe Vasilca" as this year the award was won by a young member of our team, eng. George Ghiocel Ojoc, PhD.

REFERENCES

[1] J. Donea, A. Huerta, J.-Ph. Ponthot & A. Rodrıguez-Ferran, Chapter 14. Arbitrary Lagrangian–Eulerian Methods, In Stein, E., de Borst R. & Hughes T. J. R. (Eds.), *Encyclopedia of Computational Mechanics, Volume 1: Fundamentals*, John Wiley & Sons, Ltd, 2004.
[2] W. F. Hosford, *Mechanical Behavior of Materials*, (2nd ed.), Cambridge University Press, UK, 2010.
[3] H.-H. Lee, *Finite Element Simulations with ANSYS Workbench 2021*, SDC Publications. USA, 2021.
[4] M. A. Meyers, *Dynamic Behavior of Materials*, John Wiley & Sons, Inc., USA, 1994.
[5] * * * *1200 g/m^2 Quadriaxial Stitched Glass Fabric (0°/+45°/90°/-45°), 127 cm wide* (accessed 12.01.2022), https://www.castrocompositesshop.com/en/fibre-reinforcements/1204-1200-gm2-quadriaxial-stitched-glass-fabric-0%C2%BA45%C2%BA90%C2%BA-45%C2%BA-127-cm-wide.html
[6] * * * Sika Group, About us (accessed 3.10.2021), https://www.sika.com/en/home.html
[7] V. V. Jinescu, *Application in Mechanical Engineering of Principle of Critical Energy*, Lambert Academic Publishing, Saarbrücken, Germany, 2015.
[8] A. Wiśniewski & M. Gmitrzuk, *Validation of numerical model of the Twaron CT709 ballistic fabric*, Proceedings of 27th International Symposium on Ballistics, BALLISTICS 2013, 2, 1535-1544, 2013.
[9] Y. Xie, T. Wang, L. Wang, Y. Yang, X. Sha, Numerical investigation of ballistic performance of SiC/TC4/UHMWPE composite armor against 7.62 mm AP projectile, *Ceramics International* **48**, 24079–24090, 2022.
[10] * * * *ANSYS Explicit Dynamics Analysis Guide*, ANSYS, Inc., USA, 2021.
[11] V. V. Jinescu, V.–I. Nicolof, A. Chelu, S. – E. Manea, Calculation of the local critical state taking into account the deterioration and the residual stresses, *Journal of Engineering Sciences and Inovation*, **2**, Issue 3, pp. 9-21, 2017.
[12] S. Ingle, C. S. Yerramalli, A. Guha & S. Mishra, Effect of material properties on ballistic energy absorption of woven fabrics subjected to different levels of inter-yarn friction, *Composite Structures*, **266**, 113824. doi: 10.1016/j.compstruct.2021.113824, 2021.
[13] C. S. Meyer, D. J. O'Brien, (Gama) B. Z. Haque, Jr. J. W. Gillespie, Mesoscale modeling of ballistic impact experiments on a single layer of plain weave composite, *Composites Part B*, **235**, 109753. https://doi.org/10.1016/j.compositesb.2022.109753, 2022.
[14] M. Grujicic, J. Snipes, S. Ramaswami, V. Avuthu, Unit-cell-based derivation of the material models for armor-grade composites with different architectures of ultra-high molecular-weight polyethylene fibers, *International Journal of Structural Integrity*, **7**(4), 458-489, doi: 10.1108/IJSI-06-2015-0015, 2016.
[15] G. R. Johnson & W. H. Cook, Fracture characteristics of three metals subjected to various strains, strain rates, temperatures and pressures, *Engineering Fracture Mechanics*, 21, 31-48, 1985.
[16] T. Børvik, S. Dey & A. H. Clausen, Perforation resistance of five different high-strength steel plates subjected to small-arms projectiles, *International Journal of Impact Engineering*, **36**, 948-964, doi: 10.1016/j.ijimpeng.2008.12.003, 2009.
[17] M. Giglio, A. Gilioli, A. Manes, L. Peroni & M. Scapin, Investigation about the influence of the mechanical properties of lead, *EPJ Web of Conferences*, **26**, 04010, doi: 10.1051/epjconf/20122604010, 2012.
[18] L. Peroni, M. Scapin, C. Fichera, A. Manes & M. Giglio, Mechanical properties at high strain-rate of lead core and brass jacket of a NATO 7.62 mm ball bullet in numerical simulations of ballistic impacts, in *Proceedings of DYMAT 2012*, 2012.
[19] * * * *Cohesive Zone Material (CZM) Model, Release 18.2* - © *ANSYS*, Inc. https://www.mm.bme.hu/~gyebro/files/ans_help_v182/ans_thry/thy_mat11.html